An Above-room-temperature Ferroelectric Two-Dimensional Halide Double Perovskite with Direction Dependent Properties

Shubham Ajaykumar Rajput,[a] Sudhadevi Antharjanam,[b] and Aravind Kumar Chandiran*[a]

[a]Department of Chemical Engineering, Indian Institute of Technology Madras, Adyar, Chennai, Tamil Nadu, India 600036.

[b]Sophisticated Analytical Instrument Facility, Indian Institute of Technology Madras, Adyar, Chennai, Tamil Nadu 600036, India

*aravindkumar@iitm.ac.in

Electronic Supplementary Information

Experimental Methods

Chemicals used. 3-chloropropylamine hydrochloride (Cl(CH$_2$)$_3$NH$_2$.HCl, 98%, Alfa Aesar), antimony (III) chloride (SbCl$_3$, 99%, Alfa Aesar), silver(I) oxide (Ag$_2$O, 99%, Sigma Aldrich), hydrobromic acid (HBr, ~47% in water, Spectrochem) and 1,1,2,2-tetrachloroethane (C$_2$H$_2$Cl$_4$, 98%, Spectrochem) were procured for synthesis, and all these chemicals were used without any further purification.

Synthesis of non-centrosymmetric 2D halide double perovskite. The stoichiometric mixture of 3-chloropropylamine hydrochloride (2 mmol), silver(I) oxide (0.25 mmol) and antimony (III) chloride (0.5 mmol) were dissolved in 2 ml of HBr, under continuous stirring at 100 °C for 1 hour, to achieve the clear solution. This solution was then slowly cooled to room temperature, to obtain the millimetre-sized yellow crystals of Cl$_{0.26}$Br$_{3.74}$PA$_4$AgSbBr$_8$ (CPAS, PA-propylamine). For single crystal X-ray diffraction studies, these crystals were extracted from the mother liquor and used directly for measurements. For all other characterization, the crystals were filtered, washed with 1,1,2,2-tetrachloroethane, and then dried in the hot air oven at 70 °C for 12 hours. The samples were grounded with mortar and pestle to obtain uniform powders.

Structural characterization. Single crystal X-ray diffraction (SXRD) analysis was carried out at a temperature of 25 ˚C, on Bruker D8 VENTURE single-crystal X-ray diffractometer equipped with Mo Kα X-ray radiation (λ = 0.71073 Å) source and PHOTON II detector to collect the phase and crystal structure data of CPAS. The collected data was resolved and refined using WINGX-SHELX software,[1–3] and then a CIF check was carried out on IUCR. The crystal structure was drawn using VESTA, version-3 software. Powder XRD (PXRD) measurements were performed on a Thermo Equinox 3000 X-ray powder diffractometer with a Cu-Kα source. JASCO 6600FV spectrometer fitted with ATR setup was used for FTIR measurements, operated under vacuum. Raman spectra were collected from Horiba - Yvon (HR-800UV) micro-Raman spectrometer with a 632 nm laser excitation source equipped with an 1800 gr/mm diffraction grating.

Thermal stability analysis. The thermogravimetric analysis (TGA) was performed using the SDT Q600 instrument in a nitrogen (100 mL.min^{-1}) atmosphere in the temperature range of 30 °C – 900 °C at a heating rate of 10 °C min^{-1}. Differential scanning calorimetric (DSC) measurement was

performed on NETZSCH DSC 204F1 Phoenix with a 10 °C.min^{-1} heating rate, in a nitrogen atmosphere. The reference used in the DSC study was an Al crucible with a pierced lid.

Optical measurements. The absorption spectra of the powdered material were obtained on a Shimadzu 2600 spectrophotometer equipped with a barium sulfate-coated integrating sphere. Room temperature steady-state emission and excitation spectra were recorded using Horiba Fluorolog Spectrofluorometer (Flurolog-3) containing a 450 W xenon arc lamp. To avoid second-order diffraction in the emission, suitable long-pass cut-off filters were used at the entry port of the emission monochromator. Lifetime measurements were also conducted on the same equipment with a 401 nm nanoLED laser diode with a pulse duration of less than 200 ps. The obtained data were fitted by Horiba Datastation software. The photoluminescence quantum yield (PLQY) was performed using Horiba (IS236A-4) with a 2-inch integrating sphere with four ports (K-Sphere, Horiba). The measured emission and excitation spectra for blank and sample were compared with the existing standard sample data, rhodamine 6G in water (PLQY = 0.95). More details about the experimental details of excitation spectra are provided in reference [4]. The colour coordinates are specified by Commission International de L' Eclairage (CIE-1931) chromaticity coordinates and are calculated on a chromaticity diagram. These colour coordinates are calculated from the PL emission spectra on the Horiba Fluorolog Spectrofluorometer (Flurolog-3).

Polarization-electric field (P-E) hysteresis. The P-E hysteresis loop was carried out on the CPAS single crystals in different crystal configurations using the aixACCT Systems GmbH (Aachen Germany) TF Analyzer 3000. The TF Analyzer was fitted with 150 V inbuilt amplifier and externally attached with Trek 1 kV/10 kV amplifier, connected to the Thin Film Sample Holder (TFSH) unit with high voltage extension. The samples were prepared on microscopic glass slides using the single crystals of CPAS, and contacts were made using the conductive silver paste. The tungsten wire probes (American Probe & Technologies, Inc.) with a radius of 1 μm were used in the TFSH Unit and were mounted with utmost care to make contact with the single crystals without breaking them. The optical images of the single crystals were captured using a USB microscope camera (The Imaging Source Europe GmbH - Germany) attached to the TFSH Unit. The P-E loop was measured using the triangular waveform for the CPAS single crystals.

Atomic force microscopy (AFM) and piezoresponse force microscopy (PFM) studies. The atomic force microscopy (AFM) studies were carried out on the CPAS single crystal using the Oxford Instruments (Asylum Research, Santa Barbara, CA) MFP-3D Origin+ AFM. For analyzing the piezoelectric behaviour of the single crystal, resonant enhanced piezoelectric force microscope (PFM) mode was used. All AFM and PFM measurements were measured using Pt/Ir coated cantilevers with a spring constant of 1.7 N/m and a resonance frequency of ~61 kHz.

Impedance spectroscopy. The impedance measurements were conducted on CPAS single crystals at room temperature in different crystal configurations using a Solartron Impedance/gain Phase Analyzer SI 1260, connected to Solartron 1296 Dielectric Interface. Lake Shore Cryotronics (JANIS research company) STVP-200LN-SOL cryostat was used for the temperature dependent

conductivity studies on the 8 mm diameter pellet. The impedance data was acquired in the 1 MHz – 100 mHz frequency range with an AC bias of 300 mV.

Table S1. Single crystal structural information of CPAS taken at room temperature (RT, 25 °C).

Material	$Cl_{0.26}Br_{3.74}PA_4AgSbBr_8$ (CPAS - RT)
Empirical formula	C12 H36 Ag Br11.74 Cl0.26 N4 Sb
Formula weight (g.mol^{-1})	1413.23
Temperature (K / °C)	298(2) / 25
Wavelength (Å)	0.71073
Crystal system	Monoclinic
Space group	Pc
Unit cell dimensions (Å)	a = 8.6321(12), α = 90°
	b = 7.8942(13), β = 90.1(6)°
	c = 25.961(4), γ = 90°
Volume (Å^3)	1769.1(5)
Z	2
Density (calculated) (Mg/m^3)	2.653
Absorption coefficient (mm^{-1})	14.601
F(000)	1298
Crystal size (mm^3)	0.261 x 0.167 x 0.033
Theta range for data collection	2.485 to 25.495°
Index ranges	-10<=h<=10, -9<=k<=9, -31<=l<=31
Reflections collected	51625
Independent reflections	6548 [R(int) = 0.0692]
Completeness to theta = 25.242°	99.9 %
Absorption correction	Semi-empirical from equivalents
Max. and min. transmission	0.7461 and 0.3220
Refinement method	Full-matrix least-squares on F^2
Data / restraints / parameters	6548 / 513 / 350
Goodness-of-fit on F^2	1.072
Final R indices [I>2sigma(I)]	R1 = 0.0530, wR2 = 0.1101
R indices (all data)	R1 = 0.0675, wR2 = 0.1196
Extinction coefficient	n/a
Largest diff. peak and hole (e.Å^{-3})	0.974 and -1.536

Table S2. Octahedral bond length distortion (Δd) and bond angle variance ($\sigma^2_{oct.}$) for the CPAS (at RT).

Material	Octahedral bond length distortion (Δd)		Octahedral bond angle variance ($\sigma^2_{oct.}$)	
	Sb octahedra	Ag octahedra	Sb octahedra	Ag octahedra
CPAS	6.66×10^{-4}	82.35×10^{-4}	10.38	50.18

Table S3. Two-Dimensional (2D) layered halide perovskites ferroelectrics with their optical and ferroelectric properties.

Sr. no	Material	Space group	Bandgap (eV)	P_s ($\mu C.cm^{-2}$)	T_c (K)	Ref.
1.	BZA_2PbCl_4	$Cmc2_1$	3.65	13	438	[5]
2.	$FBZA_2PbCl_4$	$Cmc2_1$	3.62	5.35	448	[6]
3.	BA_2PbCl_4	$Cmc2_1$	3.44	2.1	328	[7]
4.	$EA_4Pb_3Cl_{10}$	$Cmc2_1$	3.39	4.5	415	[8]
5.	BPA_2PbBr_4	$Cmc2_1$	2.95	4.8	375	[9]
6.	$DFCHA_2PbI_4$	$Cmc2_1$	2.38	4.5	377	[10]
7.	$DFPD_2PbI_4$	$Aba2$	2.24	10	428.5	[11]
8.	$CPA_4AgBiBr_8$	Pc	2.69	3.2	305	[12]
9.	$Cl_{0.97}Br_{3.03}PA_4AgBiBr_8$	Pc	2.45	~3.0	-	[13]
10.	$Cl_{0.26}Br_{3.74}PA_4AgSbBr_8$	Pc	2.48	3.4	-	This work

Table S4. Temperature dependent impedance measurements fitted R_1 and R_2 values.

Temperature (˚C)	R_1 (Ω)	R_2 (Ω)
-173	2.5×10^{10}	9.7×10^{10}
-148	1.95×10^{10}	8.5×10^{10}
-123	1.45×10^{10}	6.5×10^{10}
-98	4.00×10^{9}	3.3×10^{10}
-73	2.13×10^{9}	1.56×10^{10}
-48	1.2×10^{9}	9.8×10^{9}
-23	1.65×10^{8}	1.59×10^{9}
2	1.1×10^{8}	2.89×10^{8}
27	7.5×10^{7}	1.52×10^{8}
52	1.5×10^{6}	1.35×10^{7}
77	7.53×10^{5}	7.18×10^{6}
102	3.23×10^{5}	3.12×10^{6}

127	2.48 x 10^5	1.45 x 10^6
152	7.58 x 10^4	1.44 x 10^6
177	5.35 x 10^4	7 x 10^5

Table S5. Quantum yield value and colour coordinates of CPAS material.

Material	Quantum yield	Colour coordinates	
		x	y
CPAS	0.50	0.177	0.131

Equations:

$$\Delta d = \frac{1}{6} \sum_{i=1}^{6} \left[\frac{d_i - d}{d} \right]^2 \tag{S1}$$

Where Δd defines the octahedral bond length distortion, d_i is each B-X (B - Ag or Sb and X - Br) bond length, and d is the average of the six B-X bond lengths.

$$\sigma_{(oct.)}^2 = \sum_{i=1}^{12} \frac{(\theta_i - 90)^2}{11} \tag{S2}$$

where $\sigma_{(oct.)}^2$ defines the octahedral bond angle variance, θ_i denotes the individual Br–Ag–Br and Br–Sb–Br bond angles.

$$\tau_{avg.} = \frac{\sum_{i=1}^{n} B_i \tau_i^2}{\sum_{i=1}^{n} B_i \tau_i} \tag{S3}$$

where $\tau_{avg.}$ is the average lifetime of radiative recombination, τ_i is the lifetime of individual decay component and B_i is its corresponding amplitude.
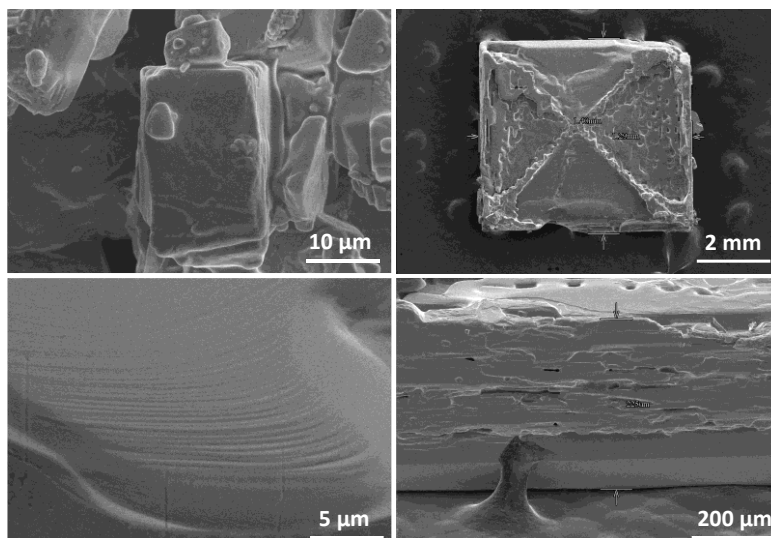
Figure S1. SEM micrographs of CPAS powder material and single crystal representing layered sheet morphology. The distribution of particle sizes in powder materials and its related explanation is provided in Figure S16.

CPAS Single crystal E-DAX

Element	Weight %	Atomic %
C	20.30	55.27
N	6.64	15.50
Cl	2.07	1.91
Br	57.13	23.38
Ag	6.34	1.92
Sb	7.51	2.02
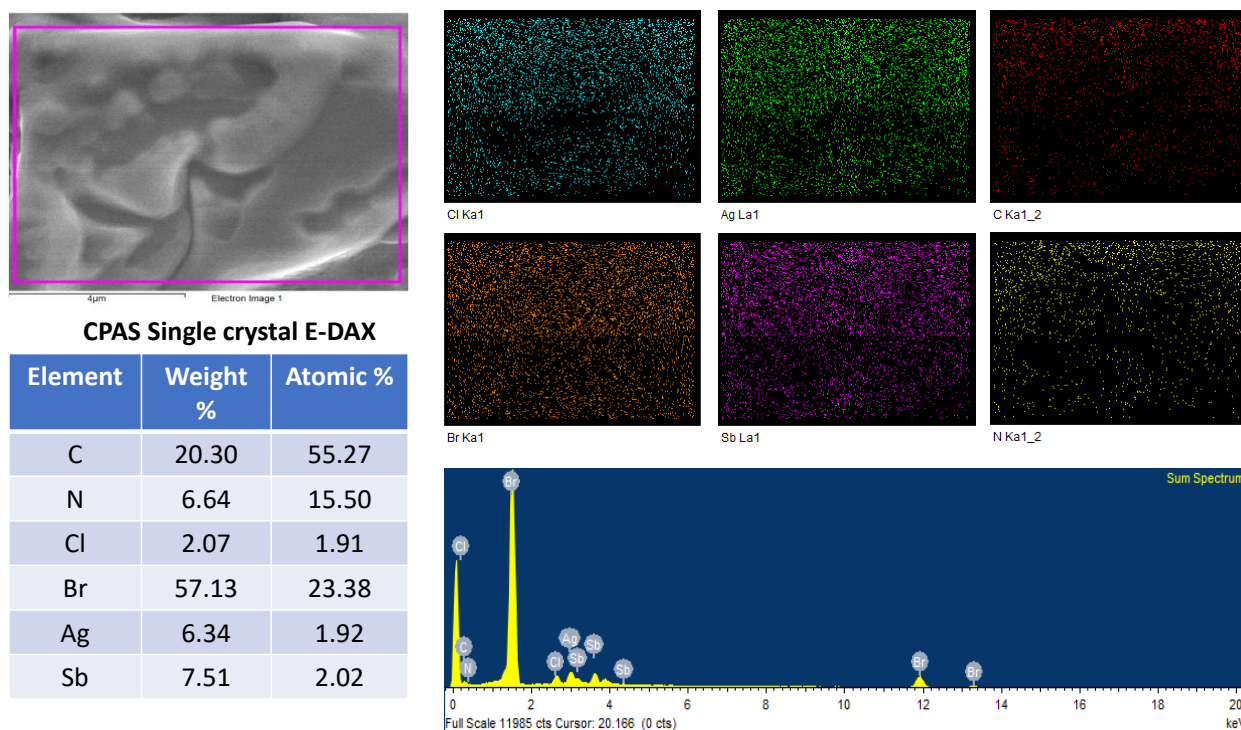
Figure S2. Energy dispersive X-ray spectroscopy (E-DAX) of CPAS single crystal.

(a)
C2'-C1-Cl1 – 127°
C2'-C1-Br9 - 144°

C8-C7'-Cl3 – 145°
C8-C7'-Br11 - 137°

(b)
C2'-C1-Cl1– 127°
C2'-C1-Br9 - 144°

C8-C7'-Cl3 – 145°
C8-C7'-Br11 - 137°
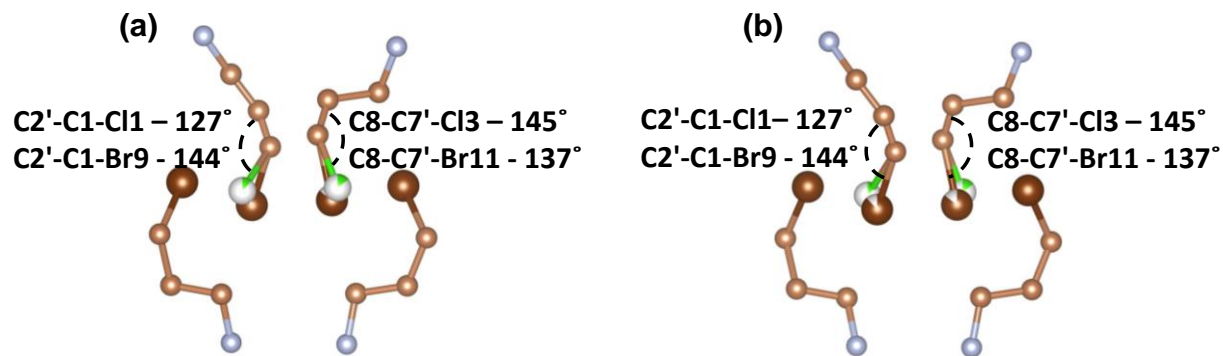
Figure S3. (a and b) represent the arrangement of the halogenated organic spacer cation in the single unit cell of CPAS at RT (25 ˚C).
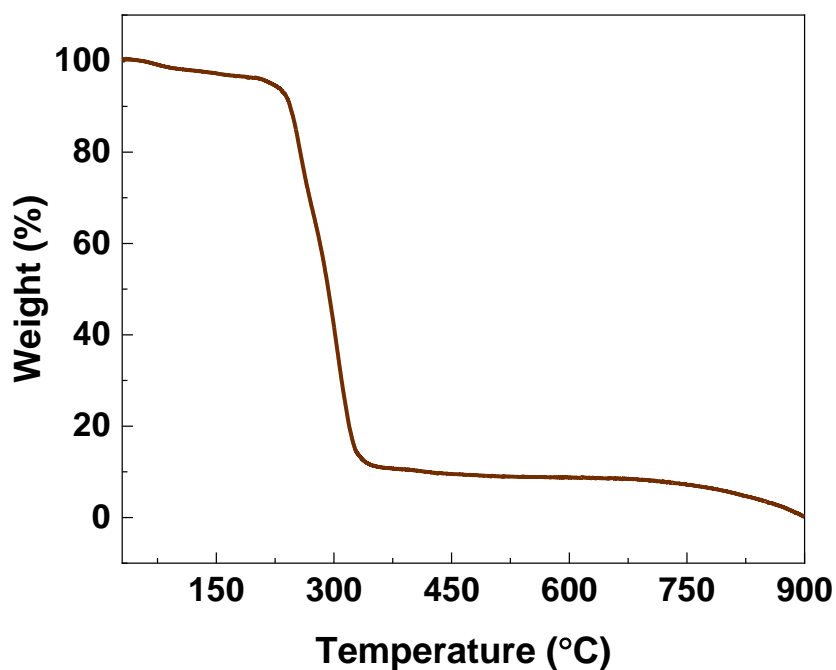
Figure S4. Thermogravimetric analysis (TGA) of CPAS powder material. The TGA results revealed that the CPAS material remained stable up to about 220 °C, with 99 % of its initial weight retained.
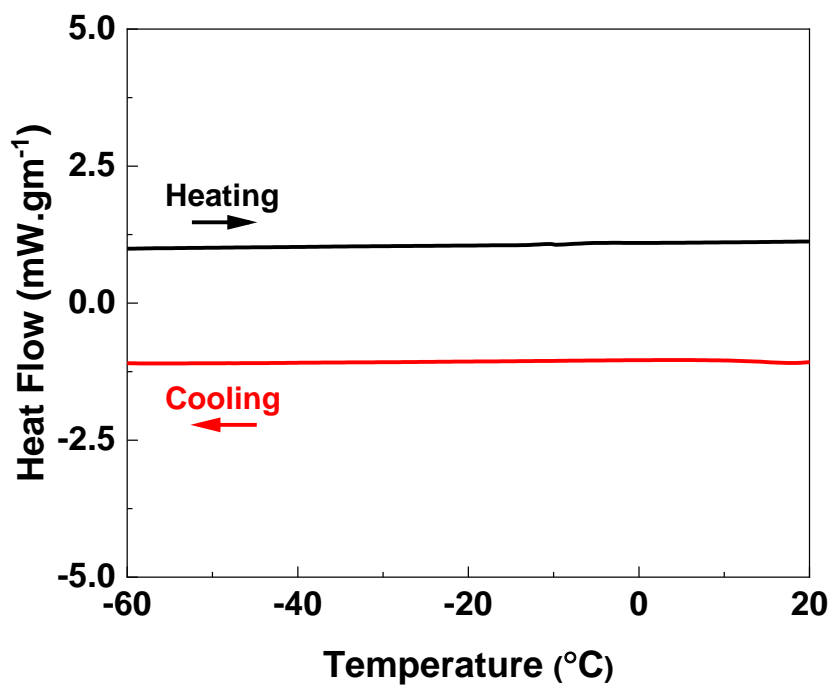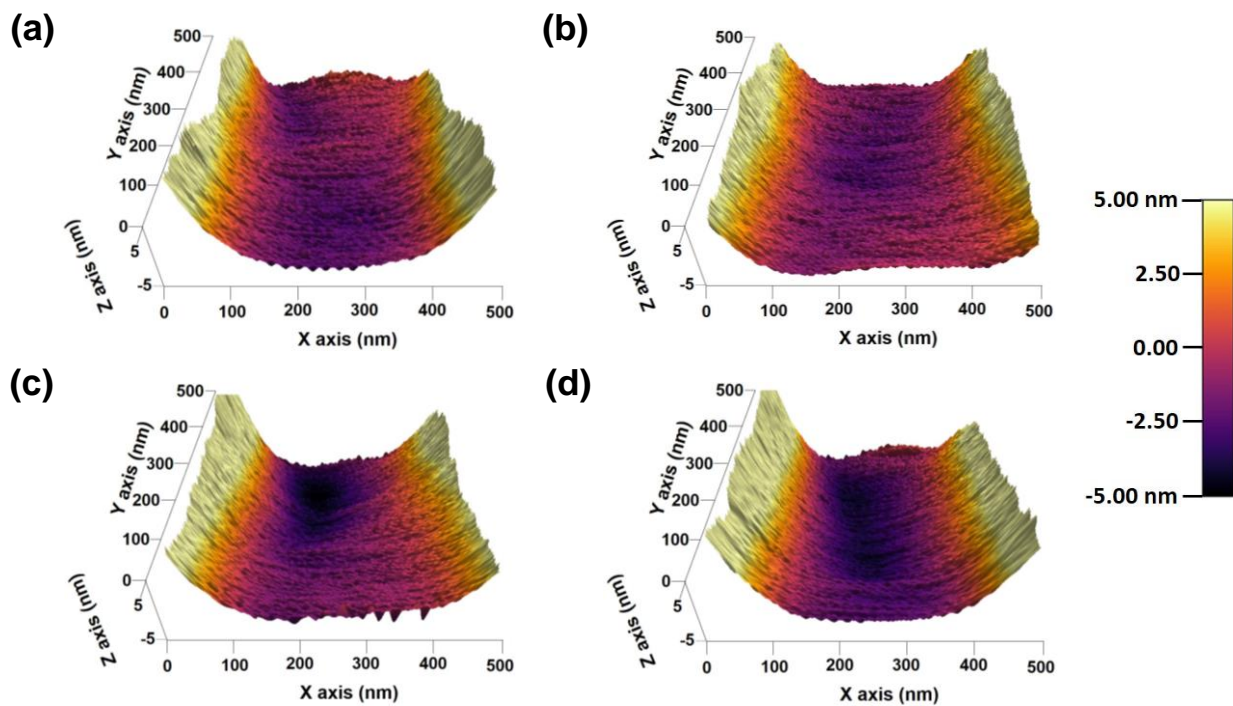
Figure S5. Differential scanning calorimetric (DSC) at low temperature (LT) representing the data of CPAS powder.
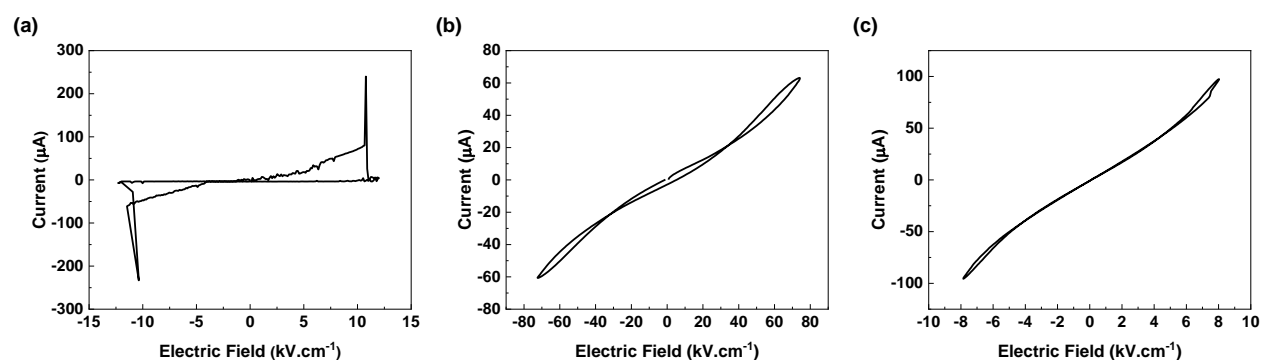

Figure S6. (a, b, and c) represents the current-electric field (I-E) curves for the perpendicular, parallel and bottom configurations of CPAS single crystals, respectively.

Figure S7. Piezoresponse force microscopy (PFM) with three-dimensional (3D) topography images of the CPAS single crystals at different applied tip voltages of (a) 1 V, (b) 2 V, (c) 3 V and (d) 4 V, showing expansion and contraction representing piezoelectric behaviour. The colour scale is given on the far right.
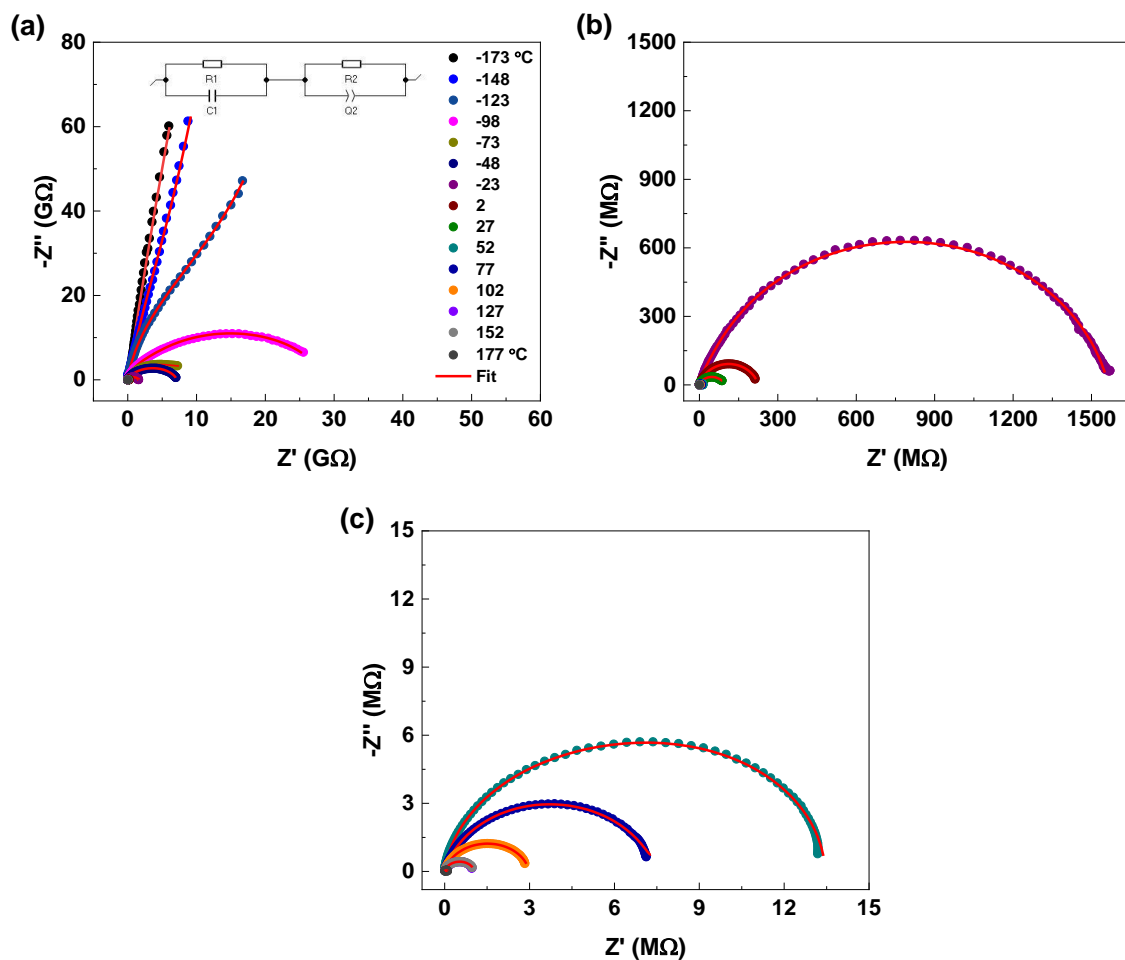
Figure S8. Temperature dependent impedance spectra of 8 mm diameter CPAS pellet with (a) representing the Nyquist plot data for the entire temperature range of -173 ˚C to 177 ˚C, and (b and c) represents zoomed-in image for the higher temperature ranges. Temperature scale in ˚C is given in (a).
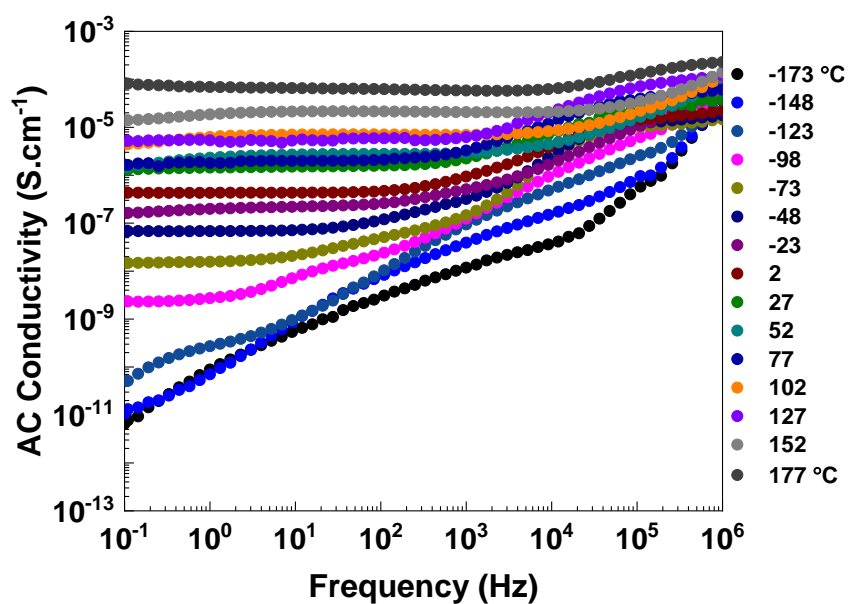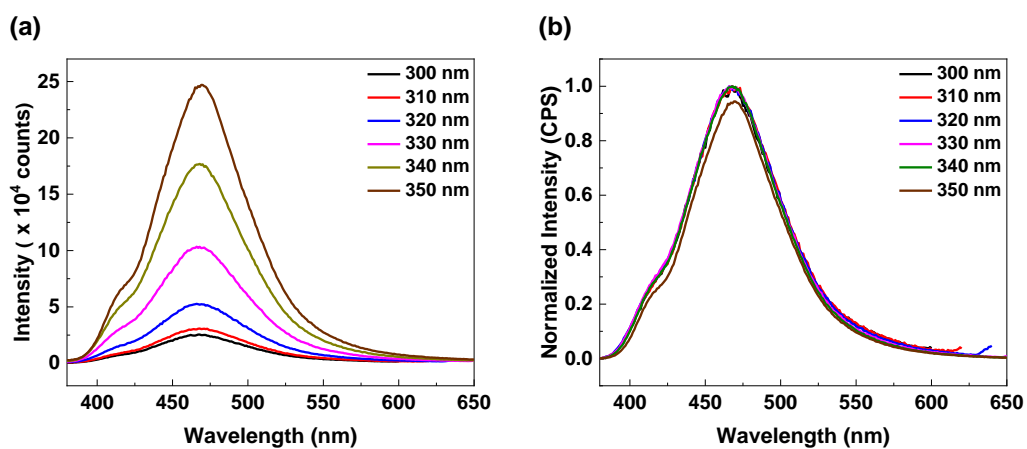
Figure S9. Variation in the AC conductivity values with frequency at different temperatures. Temperature legends in °C are given on the far right.
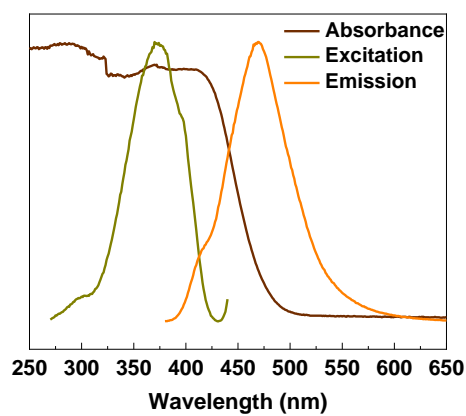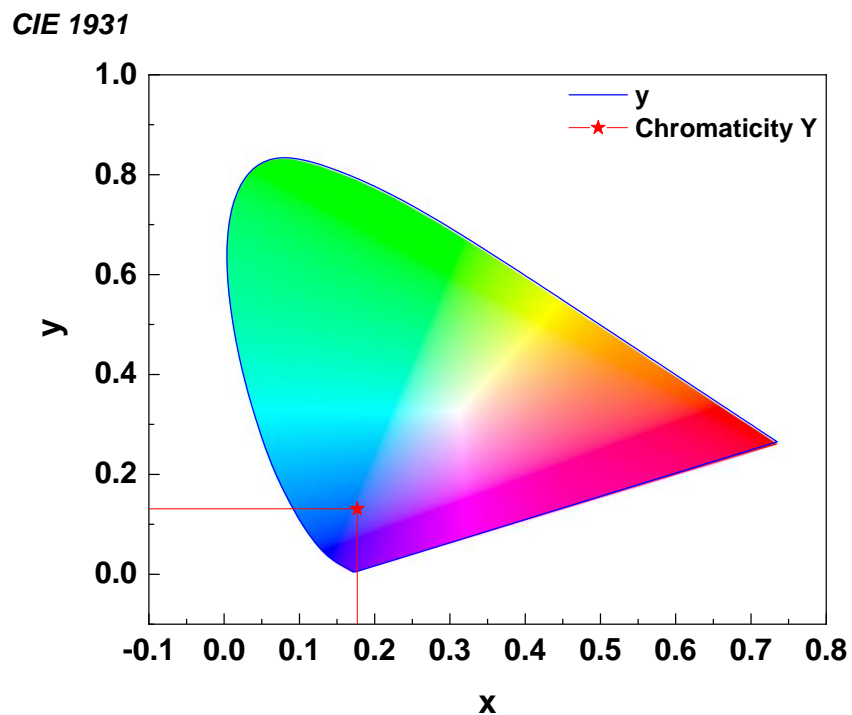

Figure S10. Absorbance, excitation and emission spectra CPAS powder sample.
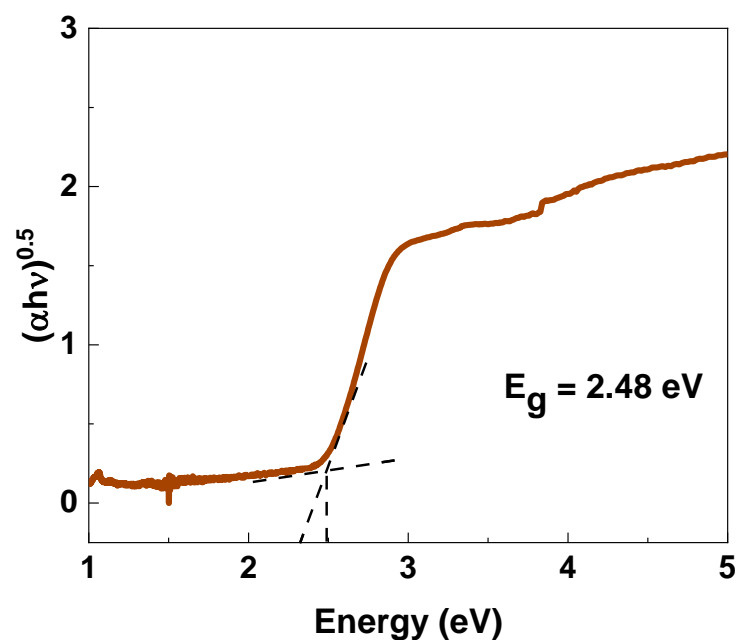
**Figure S11.** Tauc plot of the CPAS powder material.

Figure S12. (a) represents the photoluminescence emission spectra of CPAS powder sample at different excitation wavelengths, and (b) their corresponding represents the normalized spectra.

Figure S13. CIE (Commission Internationale de l'éclairage) colour coordinates x and y for the CPAS powder sample showing emission in the blue region.
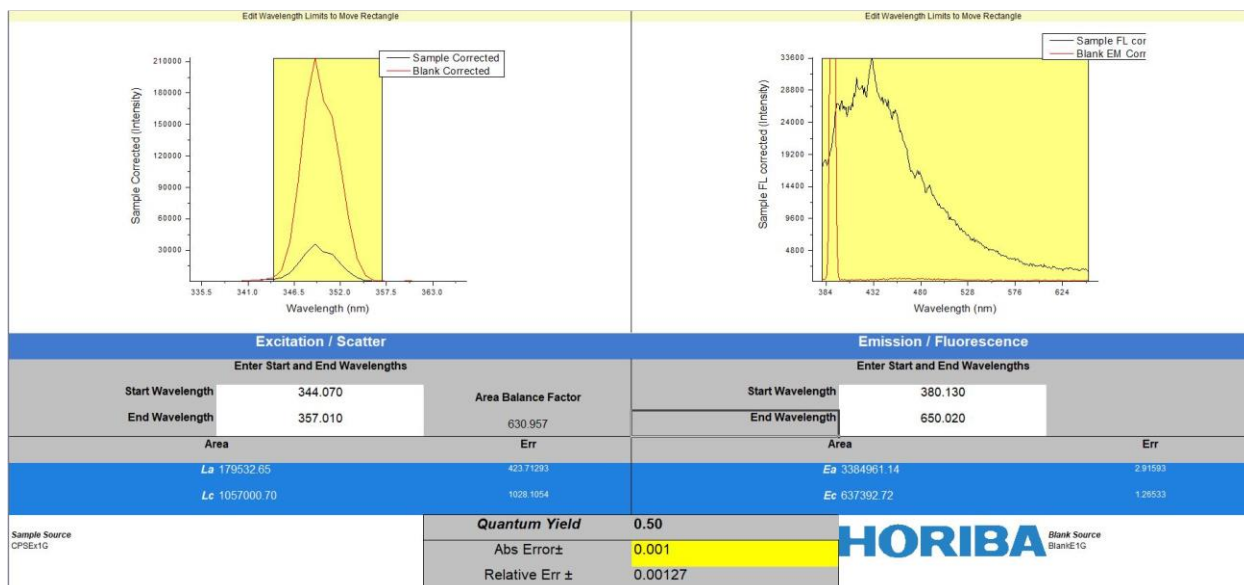

Figure S14. PLQY measurements for as-synthesized material of CPAS powder sample.
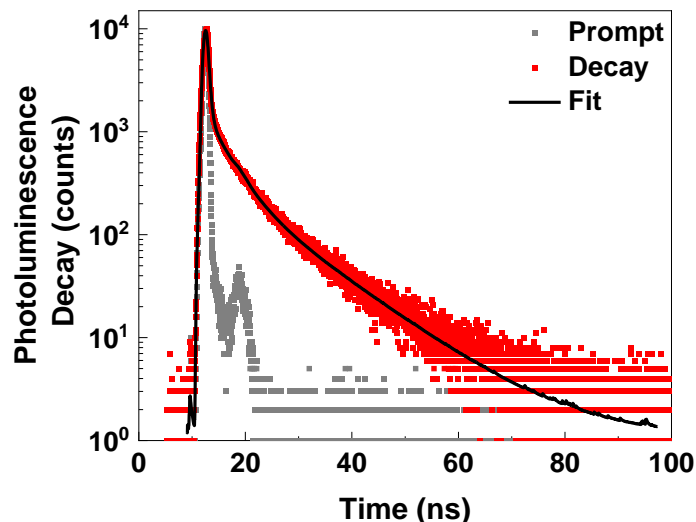
Figure S15. Time-resolved photoluminescence decay measurement. The plot was fitted using a three-exponential decay, with lifetimes of 0.33 ns (55.95 %), 3.62 ns (23.15 %) and 11.74 ns (20.90 %) when excited with 402 nm pulse laser diode. This result indicates multiple excited state electron decay pathways.

The average lifetime for the non-radiative recombination process (intensity average) can be calculated according to Equation S3. The average lifetime computed to be 2 ns for the CPAS material.
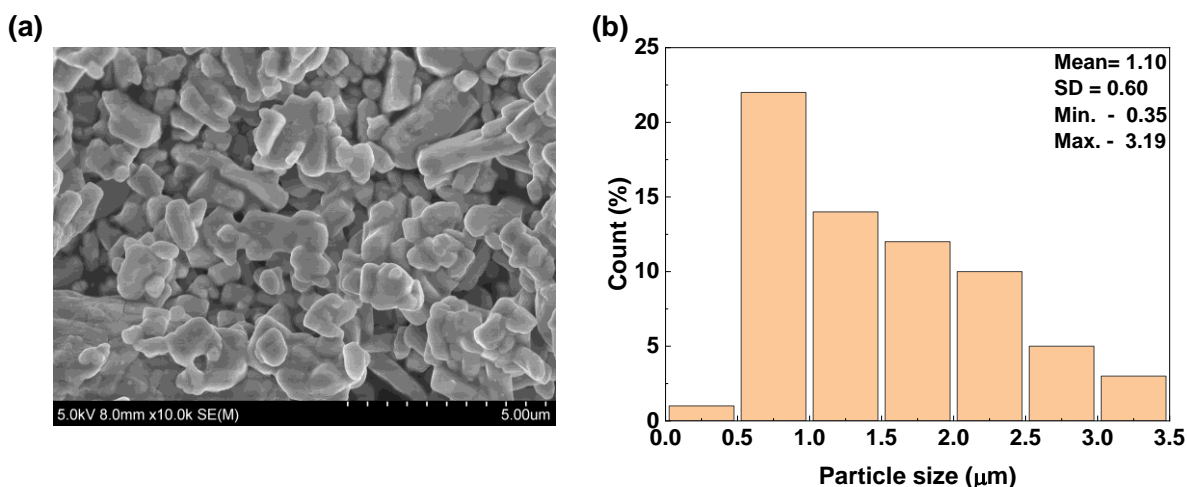
Figure S16. (a) SEM micrograph and (b) histogram of particle sizes, of CPAS material

SEM imaging at 5 μm scale of the CPAS powder material (**Figure S16(a)**) and performed particle size distribution analysis (**Figure S16(b)**) using ImageJ software.[14] The SEM micrograph reveals that the CPAS powder sample comprises of particles with layered growth pattern reminiscent of sheets, as illustrated in **Figure S1**. The histogram indicates that number of particles with sizes ranging from 0.5 to 1 μm is notably higher compared to other size ranges. Upon analysis, it was found that the minimum particle size observed is 0.35 μm, while the maximum is 3.19 μm, with a mean size of 1.10 μm and a standard deviation of 0.60 μm.

References:

1   L. J. Farrugia, *J Appl Crystallogr*, 2012, **45**, 849–854.

2   G. M. Sheldrick, *Acta Crystallogr A*, 2015, **71**, 3–8.

3   G. M. Sheldrick, *Acta Crystallogr C Struct Chem*, 2015, **71**, 3–8.

4   T. Appadurai, R. Kashikar, P. Sikarwar, S. Antharjanam, B. R. K. Nanda and A. K. Chandiran, *Commun Mater*, 2021, **2**, 68.

5   W. Q. Liao, Y. Zhang, C. L. Hu, J. G. Mao, H. Y. Ye, P. F. Li, S. D. Huang and R. G. Xiong, *Nat Commun*, 2015, **6**, 1–7.

6   P. P. Shi, S. Q. Lu, X. J. Song, X. G. Chen, W. Q. Liao, P. F. Li, Y. Y. Tang and R. G. Xiong, *J Am Chem Soc*, 2019, **141**, 18334–18340.

7   C. Ji, S. Wang, L. Li, Z. Sun, M. Hong and J. Luo, *Adv Funct Mater*, 2019, **29**, 2–7.

8   S. Wang, L. Li, W. Weng, C. Ji, X. Liu, Z. Sun, W. Lin, M. Hong and J. Luo, *J Am Chem Soc*, 2020, **142**, 55–59.

9   C. Ji, D. Dey, Y. Peng, X. Liu, L. Li and J. Luo, *Angewandte Chemie - International Edition*, 2020, **59**, 18933–18937.

10   T. T. Sha, Y. A. Xiong, Q. Pan, X. G. Chen, X. J. Song, J. Yao, S. R. Miao, Z. Y. Jing, Z. J. Feng, Y. M. You and R. G. Xiong, *Advanced Materials*, 2019, **31**, 1–7.

11   H. Y. Zhang, X. J. Song, X. G. Chen, Z. X. Zhang, Y. M. You, Y. Y. Tang and R. G. Xiong, *J Am Chem Soc*, 2020, **142**, 4925–4931.

12   W. Guo, X. Liu, S. Han, Y. Liu, Z. Xu, M. Hong, J. Luo and Z. Sun, *Angewandte Chemie - International Edition*, 2020, **59**, 13879–13884.

13   P. Siwach, P. Sikarwar, S. A. Rajput, S. Antharjanam and A. K. Chandiran, *Chemical Communications*, 2022, **58**, 10504–10507.

14   C. A. Schneider, W. S. Rasband and K. W. Eliceiri, *Nat Methods*, 2012, **9**, 671–675.